Illumination Chromaticity Estimation using Inverse-Intensity Chromaticity Space

Robby T. Tan [†] Ko Nishino [‡] Katsushi Ikeuchi [†]

[†]Department of Computer Science
The University of Tokyo
{robby,ki}@cvl.iis.u-tokyo.ac.jp

[‡]Department of Computer Science
Columbia University
kon@cs.columbia.edu

Abstract

Existing color constancy methods cannot handle both uniform colored surfaces and highly textured surfaces in a single integrated framework. Statistics-based methods require many surface colors, and become error prone when there are only few surface colors. In contrast, dichromatic-based methods can successfully handle uniformly colored surfaces, but cannot be applied to highly textured surfaces since they require precise color segmentation. In this paper, we present a single integrated method to estimate illumination chromaticity from single/multi-colored surfaces. Unlike the existing dichromatic-based methods, the proposed method requires only rough highlight regions, without segmenting the colors inside them. We show that, by analyzing highlights, a direct correlation between illumination chromaticity and image chromaticity can be obtained. This correlation is clearly described in "inverse-intensity chromaticity space", a new two-dimensional space we introduce. In addition, by utilizing the Hough transform and histogram analysis in this space, illumination chromaticity can be estimated robustly, even for a highly textured surface. Experimental results on real images show the effectiveness of the method.

1. Introduction

The spectral energy distribution of light reflected from an object is the product of illumination spectral energy distribution and surface spectral reflectance. As a result, the color of an object observed in an image is not the actual color of the object's surface. Recovering the actual surface color require the capability to discount the color of illumination. A computational approach to recover the actual color of objects is referred to as a color constancy algorithm.

Many algorithms for color constancy have been proposed. Finlayson et al. [8] categorized them into two classes: statistics-based and physics-based methods. Statistics-based methods usually relate color distribution and statistical knowledge of common lights and surfaces [2, 4, 6, 19, 22, 24]. One drawback of these methods is their requirement that many colors be observed on the target surfaces. On the other hand, physics-based methods [3, 5, 10, 15, 16], which base their algorithms on understanding the physical process of reflected light, can successfully deal with fewer surface colors, even to the extreme of a single surface color [8, 9]. Geusebroek et al. [12, 11] proposed a physical basis of color constancy by considering the spectral and spatial derivatives of the Lambertian image formation model. Andersen et al. [1] provided an analysis on object chromaticity under two illumination colors. Since our aim is to develop an algorithm that is able to handle both a single and multiple surface colors, in this section, we will concentrate our discussion on the existing physics-based methods, particularly dichromatic-based methods.

Methods in dichromatic-based color constancy rely on the dichromatic reflection model proposed by Shafer [20]. Klinker et al. [13] introduced a method to estimate illumination color from a uniform colored surface, by extracting a T-shape color distribution in the RGB space. However, in real images, it becomes quite difficult to extract the T-shape due to noise, making the final estimate unreliable.

Lee [15] introduced a method to estimate illumination chromaticity using highlights of at least two surface colors. The estimation is accomplished by finding an intersection point of two or more dichromatic lines in the chromaticity space. While this simple approach based on the physics of reflected light provides a handy method for color constancy, it suffers from a few drawbacks. First, to create the dichromatic line for each surface color from highlights, one needs to segment the colors of the highlights. This color segmentation is difficult when dealing with highly textured surfaces. Second, the estimation of illumination chromaticity becomes unstable when the surface colors are similar. Third, the method does not deal with uniformly colored surfaces. Parallel to this, several methods have been proposed in the literature [3, 21, 23, 18].

Recently, two methods have been proposed which extend Lee's algorithm [15]: Finlayson et al. [7], proposed imposing a constraint on the colors of illumination. This constraint is based on the statistics of natural illumination colors, and improves the stability in obtaining the intersection point, i.e., it addresses the second drawback of Lee's

method. Furthermore, Finlayson et al. [8] proposed the use of the Planckian locus as a constraint to accomplish illumination estimation from uniformly colored surfaces. This Planckian locus constraint on the illumination chromaticity makes the estimation more robust, especially for natural scene images. However, the method still has a few drawbacks. First, the position and the shape of the Planckian locus in chromaticity space make the estimation error prone for certain surface colors, such as bluish, yellowish, and reddish colors. Second, as they include diffuse regions in obtaining dichromatic lines, the result can become inaccurate. While the fact that their method does not require reflection separation is one of the advantages, the diffuse cluster usually has a different direction from the specular cluster; as a result, the dichromatic line can be shifted from the correct one. Third, like the previous methods, for multicolored surfaces, color segmentation is required.

In this paper, our goal is to accomplish illumination chromaticity estimation for single/multi- colored surfaces without using color segmentation. To achieve this goal, we develop a novel method based on the dichromatic reflection model, which uses highlights as a main source to analyze. Unlike previous dichromatic-based methods, the method does not require any color segmentation, thus it is applicable even for highly textured surfaces. We set our analysis on specular regions that can be easily obtained with a simple thresholding of the intensity values. This ability to work on rough estimates of highlight regions is one of the advantages of our method. Moreover, the method can handle all possible colors of illumination, since we do not make assumptions on the illumination chromaticity. Also, the method is camera-independent, as no intrinsic camera characteristics are required. Along with the new method, we introduce a new space, inverse-intensity chromaticity space, in which the correlation between image chromaticity and illumination chromaticity can be characterized.

The rest of the paper is organized as follows: in Section 2, the reflection model of inhomogeneous materials and image color formation is discussed. In Section 3, we explain the method in detail, describing the derivation of the theory and the algorithm for estimating illumination chromaticity. We provide a brief description of the implementation, experimental results and the evaluations for real images in Section 4. Finally in Section 5, we conclude our paper.

2 Reflection Model

Surface reflection of dielectric inhomogeneous objects can be described with the dichromatic reflection model, which states that the light reflected from an object is a linear combination of diffuse and specular reflections:

$$I(\lambda, \bar{\mathbf{x}}) = w_d(\bar{\mathbf{x}}) S_d(\lambda, \bar{\mathbf{x}}) E(\lambda, \bar{\mathbf{x}}) + w_s(\bar{\mathbf{x}}) S_s(\lambda, \bar{\mathbf{x}}) E(\lambda, \bar{\mathbf{x}}) \quad (1)$$

where $\bar{\mathbf{x}} = \{r, s, t\}$ is the position of a surface point in a three-dimensional world coordinate system; $w_d(\bar{\mathbf{x}})$ and $w_s(\bar{\mathbf{x}})$ are the weighting factors for diffuse and specular reflection, respectively; their values depend on the geometric structure at location $\bar{\mathbf{x}}$. $S_d(\lambda, \bar{\mathbf{x}})$ is the diffuse spectral reflectance function; $S_s(\lambda, \bar{\mathbf{x}})$ is the specular spectral reflectance function; $E(\lambda, \bar{\mathbf{x}})$ is the spectral energy distribution function of the illumination.

For most dielectric inhomogeneous objects, the spectral reflectance distribution of the specular reflection component is similar to the spectral energy distribution of the incident light [17]. Researchers usually assume that both of them are the same [8, 23, 15, 3]. Lee et al. [17] named this assumption the neutral interface reflection (NIR) assumption. As a result, we can set $S_s(\lambda, \mathbf{x})$ as a constant, and Equation (1) becomes:

$$I(\lambda, \bar{\mathbf{x}}) = w_d(\bar{\mathbf{x}}) S_d(\lambda, \bar{\mathbf{x}}) E(\lambda, \bar{\mathbf{x}}) + \tilde{w}_s(\bar{\mathbf{x}}) E(\lambda, \bar{\mathbf{x}}) \quad (2)$$

where $\tilde{w}_s(\bar{\mathbf{x}}) = w_s(\bar{\mathbf{x}}) k_s(\bar{\mathbf{x}})$, with $k_s(\bar{\mathbf{x}})$ is a constant scalar w.r.t. the wavelength.

Image Formation. An image taken by a digital color camera can be described as:

$$I_c(\mathbf{x}) = w_d(\mathbf{x}) \int_\Omega S(\lambda, \mathbf{x}) E(\lambda) q_c(\lambda) d\lambda + \tilde{w}_s(\mathbf{x}) \int_\Omega E(\lambda) q_c(\lambda) d\lambda \quad (3)$$

where $\mathbf{x} = \{x, y\}$ is the two dimensional image coordinates and q_c is the three-element-vector of sensor sensitivity and index c represents the type of sensors (R, G, and B). The integration is done over the visible spectrum (Ω). Note we ignore camera noise and gain. In addition, we assume a uniform color of illumination over the input image, so that the illumination spectral distribution $E(\lambda)$ becomes independent of the image coordinate ($\mathbf{x}$).

For the sake of simplicity, equation (3) is written as:

$$I_c(\mathbf{x}) = m_d(\mathbf{x}) \Lambda_c(\mathbf{x}) + m_s(\mathbf{x}) \Gamma_c \quad (4)$$

where $m_d(\mathbf{x}) = w_d(\mathbf{x}) L(\mathbf{x}) k_d$ with $L(\mathbf{x})$ as the spectral magnitude of the surface irradiance on a plane perpendicular to the light source direction. k_d is the scene radiance to surface irradiance ratio of diffuse surface. $m_s = \tilde{w}_s(\mathbf{x}) L(\mathbf{x})$ and $\Lambda_c = \int_\Omega s(\lambda) e(\lambda) q_c(\lambda) d\lambda$ with $s(\lambda)$ as the normalized surface reflectance spectral function and $e(\lambda)$ as the normalized illumination spectral energy distribution. Also, $\Gamma_c = \int_\Omega e(\lambda) q_c(\lambda) d\lambda$.

3. Estimation Method

Chromaticity can be defined as:

$$c(\mathbf{x}) = \frac{I_c(\mathbf{x})}{\Sigma I_i(\mathbf{x})} \quad (5)$$

where $\Sigma I_i(\mathbf{x}) = I_r(\mathbf{x}) + I_g(\mathbf{x}) + I_b(\mathbf{x})$.

In the previous section, Λ_c and Γ_c have already been defined as integral functions of the normalized surface reflectance, normalized illumination spectral and camera sensitivity. Besides these definitions, we can also define them using chromaticity. For diffuse reflection component ($m_s = 0$) Λ_c becomes equal to c, while for specular reflection component ($m_d = 0$) Γ_c equals to c. Also we can assume $\Sigma\Gamma_i = \Sigma\Lambda_i = 1$ without loss of generality. As a result, we have three types of chromaticity: image chromaticity (c), surface chromaticity (Λ_c) and illumination chromaticity (Γ_c). The image chromaticity can be directly obtained from the input image using Equation (5).

3.1 Image Chromaticity and Intensity

In this section, we analyze the three types of chromaticity to characterize the correlation between image chromaticity and intensity.

By substituting each channel's intensity in equation (5) with its definition in equation (4), the image chromaticity can be written in terms of dichromatic reflection model as:

$$c(\mathbf{x}) = \frac{m_d(\mathbf{x})\Lambda_c(\mathbf{x}) + m_s(\mathbf{x})\Gamma_c}{m_d(\mathbf{x})\Sigma\Lambda_i(\mathbf{x}) + m_s(\mathbf{x})\Sigma\Gamma_i} \quad (6)$$

By deriving the last equation we can obtain the correlation between specular and diffuse reflection coefficients (the location parameter can be removed since we are working on each pixel independently):

$$m_s = \frac{m_d(\Lambda_c - c)}{c - \Gamma_c} \quad (7)$$

Then, by plugging Equation (7) into Equation (4), the correlation between intensity and image chromaticity can be described as:

$$I_c = m_d(\Lambda_c - \Gamma_c)(\frac{c}{c - \Gamma_c}) \quad (8)$$

Figure 1.b depicts both specular and diffuse points in chromaticity-intensity space. The specular points form a curved cluster in the space, as the correlation between the values of image chromaticity (c) and intensity (I_c) are not linear.

3.2. Image Chromaticity and Illumination Chromaticity

By introducing p which we define as $p = m_d(\Lambda_c - \Gamma_c)$ and using simple algebra operations, the correlation between image chromaticity and illumination chromaticity can be derived from the Equation (8):

$$c = p\frac{1}{\Sigma I_i} + \Gamma_c \quad (9)$$

This equation is the core of our method. It shows that by knowing image chromaticity (c) and total intensity (ΣI_i), we are able to determine the illumination chromaticity (Γ_c). The details are as follows.

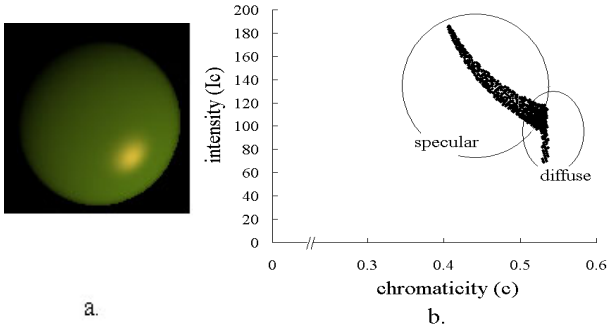

Figure 1: Synthetic image with a single surface color rendered using Torrance-Sparrow reflection model [25]. b. Projection of the diffuse and specular pixels into chromaticity-intensity space, with c representing the green channel

If the values of p are constant throughout the image, the last equation becomes a linear equation, and the illumination chromaticity (Γ_c) can be estimated in a straightforward manner by using general line fitting algorithms. However, in most images, the values of p are not constant, since p depends on the diffuse coefficient (m_d), surface chromaticity (Λ_c) and illumination chromaticity (Γ_c) itself.

For the sake of simplicity, for the moment we assume that the values of Λ_c are constant, which makes the values of p depend solely on m_d, as Γ_c has already been assumed to be constant.

According to the Lambert's Law [14], the value of m_d is determined by diffuse albedo (k_d), intensity of incident light (L), and the angle between lighting direction and surface normal. The value of diffuse albedo is constant if the surface has a uniform color. The angles between surface normals and light directions depend on the shape of the object and the light distribution; hence the angles differ for each surface point. The values of L are mostly determined by the location of illuminants, which will be constant if the locations of the illuminants are distant from the surface. However, for relatively nearby illuminants, the values of L may vary w.r.t. the surface point. As a result, in general conditions, the values of m_d vary over the entire surface.

Fortunately, for some sets of surface points, the differences of m_d are small and can be approximated as constant. We can take this approximation for granted, as current ordinary digital cameras automatically do it for us as a part of their accuracy limitation. Hence, specular pixels can be grouped into a number of clusters that have the same values of m_d. These groups can be observed in Figure 2, where it is shown that pixels with the same m_d, which means the same p, form a curved line. The number of curved lines depends on the number of different values of m_d.

Therefore, for each group of pixels that share the same value of m_d, we can consider p as a constant, which makes Equation (9) become a linear equation, with p as its constant

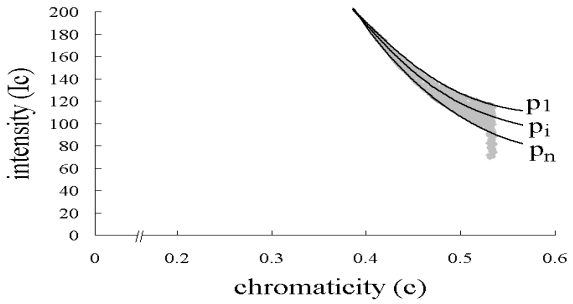

Figure 2: Enlargement of Figure 1.b, with n as the number of the variance of m_d and i is a line index, where $1 \leq i \leq n$

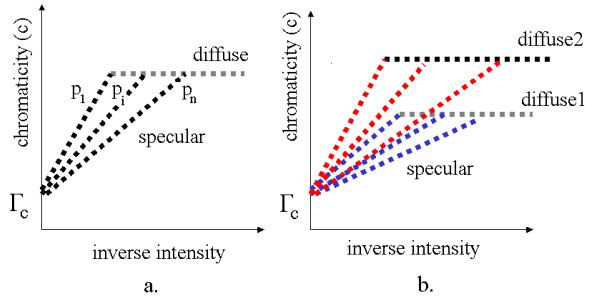

Figure 3: a. Sketch of specular points of a single surface color in inverse-intensity chromaticity space. b. Sketch of specular points of two surface colors in inverse-intensity chromaticity space.

gradient. These groups of pixels can be clearly observed in a two-dimensional space: inverse-intensity chromaticity space, with x-axis representing inverse-intensity ($\frac{1}{\Sigma I_i}$) and y-axis representing image chromaticity (c), as illustrated in Figure 3.a. Several straight lines in the space correspond to several groups of different m_d values (several number of different p: p_1,..., p_i,..., p_n). These lines intersect at a single point on the y-axis, which is identical to the illumination chromaticity (Γ_c). Figure 4.b shows the specular points of a synthetic image with a uniformly colored surface in the inverse-intensity chromaticity space.

Now we relax the assumption of uniformly colored surface to handle multicolored surfaces. Figure 3.b. illustrates the projection of two different surface colors into the inverse-intensity chromaticity space. We can observe that two clusters of straight lines with different values of surface chromaticity head for the same value on the chromaticity axis (Γ_c). Since we only consider points that have the same values of p and Γ_c, then even if there are many different clusters with different values of Λ_c, as is the case for multicolored surfaces, we can still safely estimate the illumination chromaticity (Γ_c) from the intersection with the chromaticity axis. This means that, for multicolored surfaces, the estimation process is exactly the same to the case of a uniformly colored surface. Figure 5.b shows the projection of hightlighted regions of a synthetic image with two surface colors into the inverse-intensity chromaticity space.

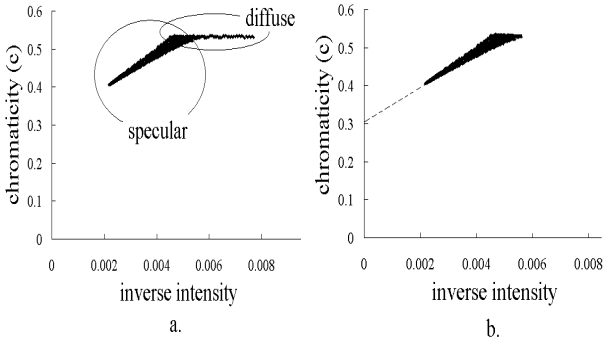

Figure 4: a. Diffuse and specular points of a synthetic image (Figure 1.a) in inverse-intensity chromaticity space, with c representing the green channel. b. The cluster of specular region only

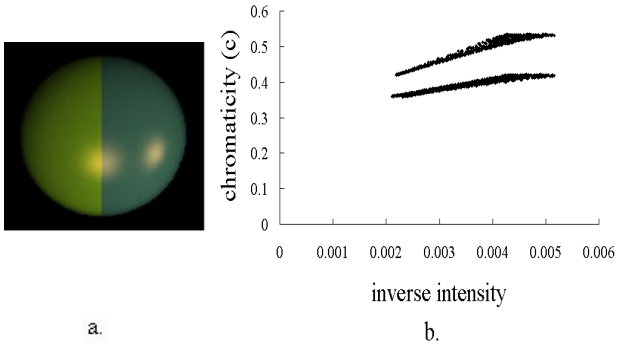

Figure 5: a. Synthetic image with multiple surface colors. b. Specular points in inverse-intensity chromaticity space, with c representing the green channel

3.3. Estimating Illumination Chromaticity

To estimate the illumination chromaticity (Γ_c) from inverse-intensity chromaticity space, we use the Hough transform. Figure 6.a shows the transformation from the inverse-intensity chromaticity space into the Hough space, where its x-axis represents Γ_c and its y-axis represents p. Since Γ_c is a normalized value, the range of its value is from 0 to 1 ($0 < \Gamma_c < 1$).

Using the Hough transform alone does not yet give any solution, because the values of p are not constant throughout the image, which makes the intersection point of lines not located at a single location. Fortunately, even if the values of p vary, the values of Γ_c are constant. Thus, in principle, all intersections will be concentrated at a single value of Γ_c, with a small range of p's values. These intersections are indicated by a thick solid line in Figure 6.a.

If we focus on the intersections in the Hough space as illustrated in Figure 6.b, we should find that larger number of intersections at a certain value of Γ_c compared to other values of Γ_c. This is due to the fact that in inverse-intensity chromaticity space, within the range of Γ_c ($0 < \Gamma_c < 1$), the number of groups of points that form a straight line heading for certain value of Γ_c are more dominant than the number of groups of points that form a straight line heading

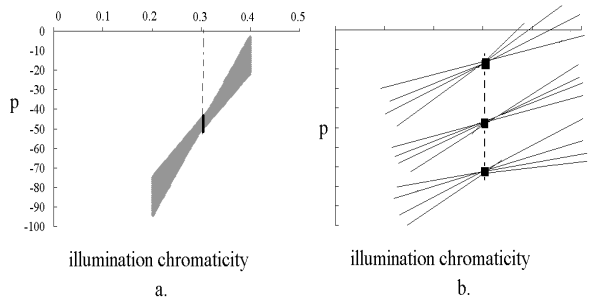

Figure 6: a. Projection of points in Figure 4.b into the Hough space. b. Sketch of intersected lines in the Hough space.

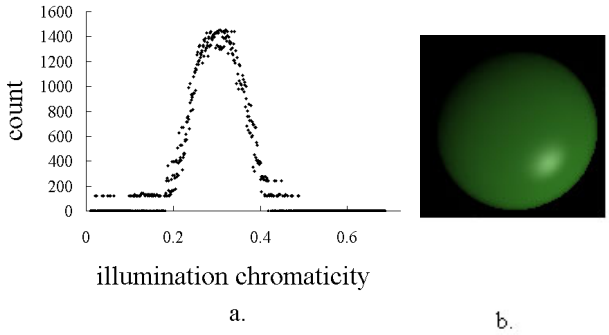

Figure 7: a. Intersection-counting distribution in the green channel of chromaticity. b. Normalization result of the input synthetic image into pure white illumination with regard to the illumination chromaticity estimation. The estimated illumination chromaticity is as follows: $\Gamma_r = 0.5354$, $\Gamma_b = 0.3032$, $\Gamma_b = 0.1618$, the ground-truth values are: $\Gamma_r = 0.5358$, $\Gamma_b = 0.3037$, $\Gamma_b = 0.1604$

for other values of Γ_c.

In practice, we count the intersections in the Hough space based on the number of points that occupy the same location. The details are as follows. A line in the Hough space is formed by a number of points. If this line is not intersected by other lines, then each point will occupy a certain location uniquely (one point for each location). However, if two lines intersect, a location where the intersection takes place will be shared by two points. The number of points will increase if other lines also intersect with those two lines at the same location. Thus, to count the intersections, we first discard all points that occupy a location uniquely, as it means there are no intersections, and then count the number of points for each value of Γ_c.

As a consequence, by projecting the total number of intersections of each Γ_c into a two-dimensional space, illumination-chromaticity count space, with y-axis representing the count of intersections and x-axis representing Γ_c, we can robustly estimate the actual value of Γ_c. Figure 7.a shows the distribution of the count numbers of intersections in the space, where the distribution forms a Gaussian-like distribution. The peak of the distribution lies at the actual value of Γ_c.

4. Experimental Results

In this section, we first briefly describe the implementation of the proposed method, then present several experimental results and show the evaluation of our experiments.

Implementation Implementation of the proposed method is quite simple. Given an image that has highlights, we first find the highlights by using intensity as an indicator. These highlight locations need not be precise; even if regions of diffuse pixels are included, the algorithm works robustly. Of course, more preciseness is better. Usually, we obtain the specular pixels from the top 55% to 65% of pixel intensities. This simple thresholding will fail if the diffuse intensities are dominantly brighter than the specular intensities, although this is rarely the case in real images. Then, for each color channel, we project the highlighted pixels into inverse-intensity chromaticity space. From this space, we use the conventional Hough transform to project the clusters into the Hough space. During the projection, we count all possible intersections at each value of chromaticity. We plot these intersection-counting numbers into the illumination-chromaticity count space. Ideally, from this space, we can choose the tip as the estimated illumination chromaticity. However, as noise always exists in real images, the result can be improved by computing the median of a certain percentage from the highest counts. In our implementation, we use 30% from the highest counted number.

Experimental Conditions We conducted several experiments on real images, which were taken using a SONY DXC-9000, a progressive 3 CCD digital camera, by setting its gamma correction off. To ensure that the outputs of the camera are linear to the flux of incident light, we used a spectrometer: Photo Research PR-650. We examined the algorithm using three types of surface, i.e., uniform colored surfaces, multicolored surfaces, and highly textured surfaces. We used convex objects to avoid interreflection, and excluded saturated pixels from the computation. For evaluation, we compared the results with the average values of image chromaticity of a white reference image (Photo Research Reflectance Standard model SRS-3), captured by the same camera. The standard deviations of these average values under various illuminant positions and colors were approximately $0.01 \sim 0.03$.

Result on a uniformly colored surface Figure 8.a shows a real image of a head model that has a uniformly colored surface and relatively low specularity, illuminated by Solux Halogen with temperature $4700K$. Under the illumination, the image chromaticity of the white reference taken by our camera has chromaticity value: $\Gamma_r = 0.3710, \Gamma_g = 0.31803, \Gamma_b = 0.3103$.

Figure 8.b shows the specular points of the red channel of chromaticity in the inverse-intensity chromaticity space. Even there is some noise, generally, all points form several

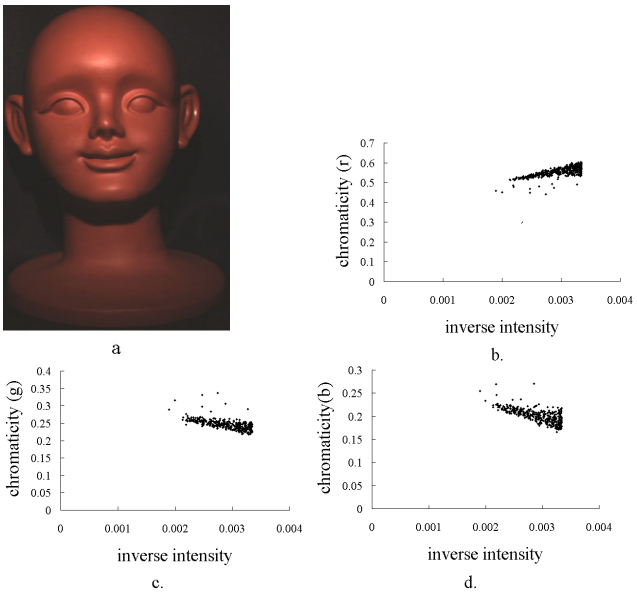

Figure 8: a. Real input image with a single surface color. b. Result of projecting the specular pixels into inverse-intensity chromaticity space, with c representing the red channel. c. Result of projecting the specular pixels, with c representing the green channel. d. Result of projecting the specular pixels, with c representing the blue channel.

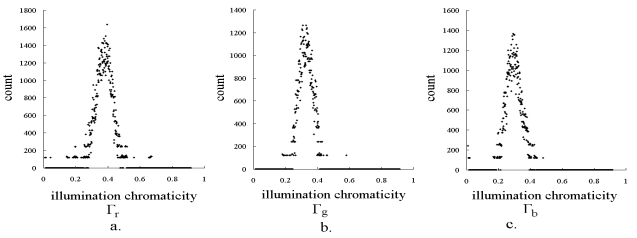

Figure 9: a. Intersection-counting distribution for red channel of illumination chromaticity in Figure 8. b. Intersection-counting distribution for green-channel c. Intersection-counting distribution for blue channel.

straight lines heading for a certain point in the chromaticity axis. The same phenomenon can also be observed in Figure 8.c and Figure 8.d. Figure 9 shows the intersection-counting distribution in the illumination-chromaticity count space. The peaks of the distribution denote the illumination chromaticity. The result of the estimation was: $\Gamma_r = 0.3779, \Gamma_g = 0.3242, \Gamma_b = 0.2866$. The error of the estimation compared with the image chromaticity of the white reference was $\epsilon_r = 0.0069$, $\epsilon_g = 0.0061$, $\epsilon_b = 0.0237$, which indicates the estimation is considerably accurate.

Result on a multi-colored surface Figure 10.a shows a plastic toy with a multicolored surface. The illumination is Solux Halogen covered with a green filter. The image chromaticity of the white reference under this illuminant taken by our camera was $\Gamma_r = 0.29804, \Gamma_g = 0.45807, \Gamma_b = 0.24387$.

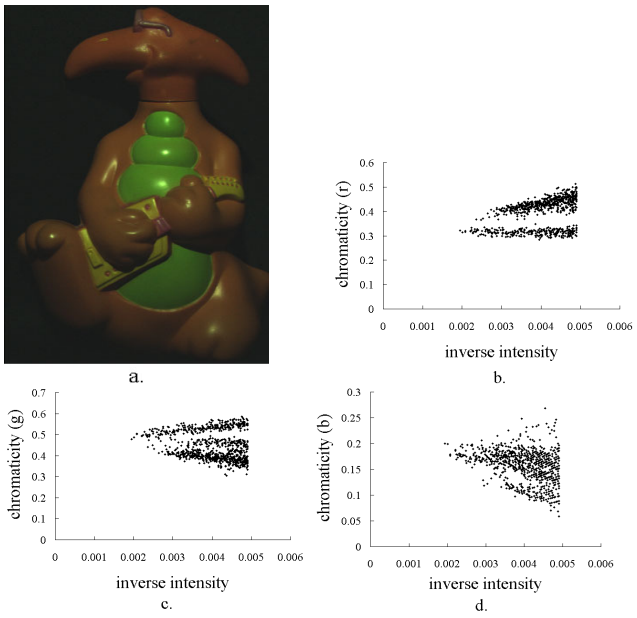

Figure 10: a. Real input image with multiples surface colors. b. Result of projecting the specular pixels into inverse-intensity chromaticity space, with c representing the red channel. c. Result of projecting the specular pixels, with c representing the green channel. d. Result of projecting the specular pixels, with c representing the blue channel.

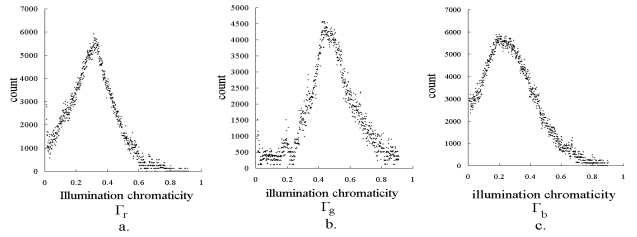

Figure 11: a. Intersection-counting distribution for the red channel of illumination chromaticity in Figure 10. b. Intersection-counting distribution for the green channel c. Intersection-counting distribution for the blue channel.

Figure 10.b, c, d show the specular points of multiple surface colors in inverse-intensity chromaticity space. From Figure 11, we can observe that, even for several surface colors, the peak of intersection counts was still at a single value of Γ_c. The result of the estimation was $\Gamma_r = 0.3194, \Gamma_g = 0.4387, \Gamma_b = 0.2125$. The error of the estimation with regard to the image chromaticity of the white reference was $\epsilon_r = 0.0213$, $\epsilon_g = 0.0193$, $\epsilon_b = 0.0317$.

Results on highly textured surface Figure 12.a shows a cover of a magazine with a highly textured surface. The illumination is Solux Halogen covered with a blue filter. The image chromaticity of the white reference under this illuminant taken by our camera has a chromaticity value of

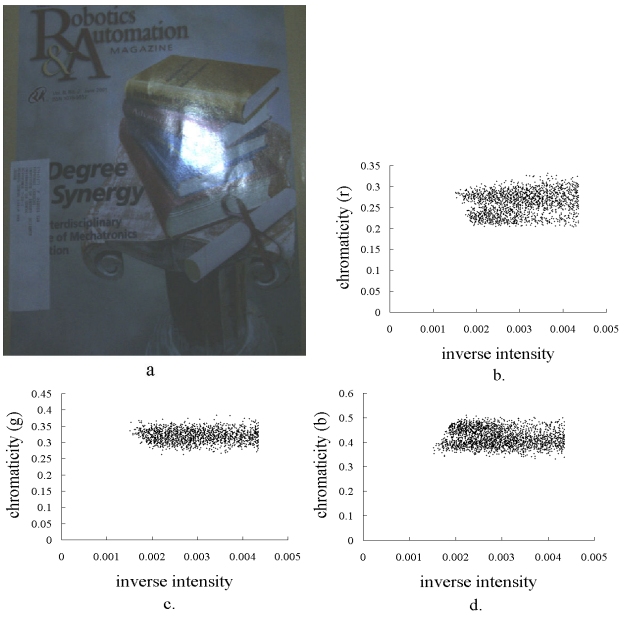

Figure 12: a. Real input image with a highly textured surface. b. Result of projecting the specular pixels into inverse-intensity chromaticity space, with c representing the red channel. c. Result of projecting the specular pixels, with c representing the green channel. d. Result of projecting the specular pixels, with c representing the blue channel.

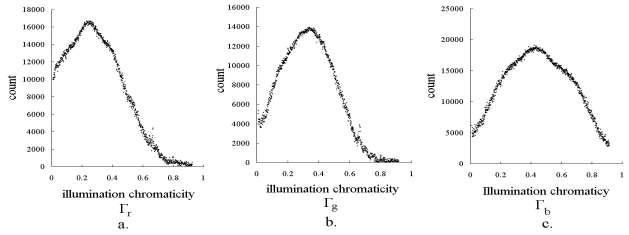

Figure 13: a. Intersection-counting distribution for red channel of illumination chromaticity in Figure 12. b. Intersection-counting distribution for green channel c. Intersection-counting distribution for blue channel.

$\Gamma_r = 0.25786, \Gamma_g = 0.31358, \Gamma_b = 0.42855$. The result of the estimation was $\Gamma_r = 0.2440, \Gamma_g = 0.3448, \Gamma_b = 0.4313$. The error of the estimation compared with the image chromaticity of the white reference was $\epsilon_r = 0.01386$, $\epsilon_g = 0.0312$, $\epsilon_b = 0.00275$.

Figure 14.a shows another magazine cover with a complex multicolored surface, which was lit by a fluorescent light covered with a green filter. The image chromaticity of the white reference under this illuminant taken by our camera has a chromaticity value of $\Gamma_r = 0.2828, \Gamma_g = 0.48119, \Gamma_b = 0.2359$. The result of the estimation was $\Gamma_r = 0.3150, \Gamma_g = 0.5150, \Gamma_b = 0.2070$. The error of the estimation compared to the image chromaticity of the white reference was $\epsilon_r = 0.0322$, $\epsilon_g = 0.03381$, $\epsilon_b = 0.0289$.

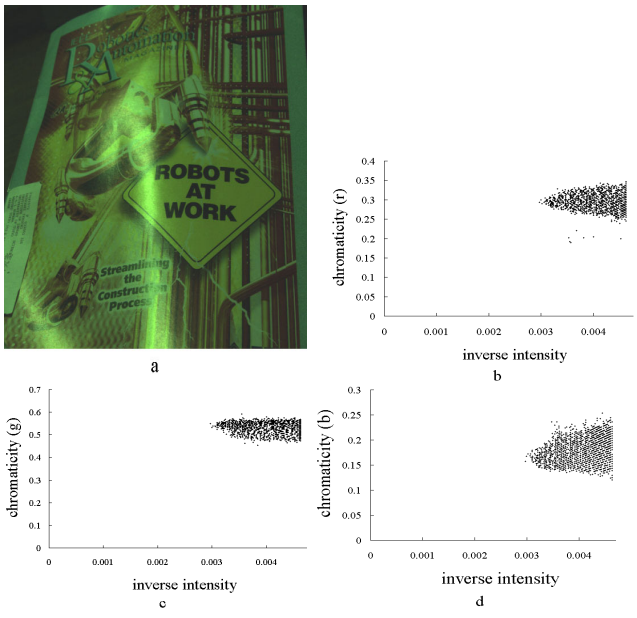

Figure 14: a. Real input image of complex multicolored surface. b. Result of projecting the specular pixels into inverse-intensity chromaticity space, with c representing the red channel. c. Result of projecting the specular pixels, with c representing the green channel. d. Result of projecting the specular pixels, with c representing the blue channel.

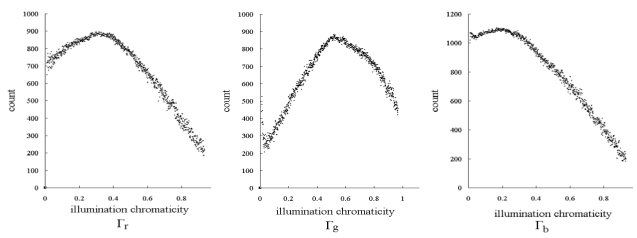

Figure 15: a. Intersection-counting distribution for the red channel of illumination chromaticity in Figure 14. b. Intersection-counting distribution for the green channel c. Intersection-counting distribution for the blue channel.

Evaluation To evaluate the robustness of our method, we have also conducted experiments on 6 different objects: 2 objects with a single surface color, 1 object with multiple surface colors, and 3 objects with highly textured surfaces. The colors of illuminants were grouped into 5 different colors: Solux Halogen lamp with temperature $4700K$, incandescent lamp with temperature around $2800K$, Solux Halogen lamp covered with green, blue and purple filters. The illuminants were arranged at various positions. The total of images in our experiment was 43 images. From these images, we calculated the errors of the estimation by comparing them with the image chromaticity of the white reference, which are shown in Table 1. The errors are considerably small, as the standard deviations of the reference image chromaticity are around $0.01 \sim 0.03$.

Table 1: The performance of the estimation method with regard to the image chromaticity of the white reference

	red	green	blue
Average of error ($\bar{\epsilon}$)	0.01723	0.01409	0.0201
Minimum error (ϵ_{min})	0.00095	0.00045	0.00021
Maximum error (ϵ_{max})	0.04500	0.04200	0.04631
Std. dev. of error (S_ϵ)	0.0106	0.01124	0.01260

5. Conclusion

We have introduced a new method for illumination chromaticity estimation.The proposed method can handle both uniform and non-uniform surface color object without requiring color segmentation. It is also applicable for multiple objects with various colored surfaces, as long as there are no interreflections. We only require a rough estimation of the specular surface regions, which can be easily obtained through simple intensity thresholding. We also introduced the *inverse-intensity chromaticity space* to analyze the relationship between illumination chromaticity and image chromaticity. Our method utilizes Hough transform and histogram analysis to robustly estimate the illumination chromaticity through this new space. There are many advantages of the method. First, the capability to cope with either single surface color or multiple surface colors. Second, color segmentation and intrinsic camera characteristics are not required. Third, the capability to deal with all possible illumination colors. The experimental results have shown that the method is accurate and robust even for highly textured surfaces.

References

[1] H.J. Andersen and E. Granum. Classifying illumination conditions from two light sources by colour histogram assessment. *Journal of Optics Society of America A.*, 17(4):667–676, 2000.

[2] D.H. Brainard and W.T. Freeman. Bayesian color constancy. *Journal of Optics Society of America A.*, 14(7):1393–1411, 1997.

[3] M. D'Zmura and P. Lennie. Mechanism of color constancy. *Journal of Optics Society of America A.*, 3(10):1162–1672, 1986.

[4] G.D. Finlayson. Color in perspective. *IEEE Trans. on Pattern Analysis and Machine Intelligence*, 18(10):1034–1038, 1996.

[5] G.D. Finlayson and B.V. Funt. Color constancy using shadows. *Perception*, 23:89–90, 1994.

[6] G.D. Finlayson, S.D. Hordley, and P.M. Hubel. Color by correlation: a simple, unifying, framework for color constancy. *IEEE Trans. on Pattern Analysis and Machine Intelligence*, 23(11):1209–1221, 2001.

[7] G.D. Finlayson and G. Schaefer. Convex and non-convex illumination constraints for dichromatic color constancy. In *Conference on Computer Vision and Pattern Recognition*, volume I, page 598, 2001.

[8] G.D. Finlayson and G. Schaefer. Solving for color constancy using a constrained dichromatic reflection model. *International Journal of Computer Vision*, 42(3):127–144, 2001.

[9] G.D. Finlayson and S.D.Hordley. Color constancy at a pixel. *Journal of Optics Society of America A.*, 18(2):253–264, 2001.

[10] B.V. Funt, M. Drew, and J. Ho. Color constancy from mutual reflection. *International Journal of Computer Vision*, 6(1):5–24, 1991.

[11] J.M. Geusebroek, R. Boomgaard, S. Smeulders, and H. Geert. Color invariance. *IEEE Trans. on Pattern Analysis and Machine Intelligence*, 23(12):1338–1350, 2001.

[12] J.M. Geusebroek, R. Boomgaard, S. Smeulders, and T. Gevers. A physical basis for color constancy. In *The First European Conference on Colour in Graphics, Image and Vision*, pages 3–6, 2002.

[13] G.J. Klinker, S.A. Shafer, and T. Kanade. The measurement of highlights in color images. *International Journal of Computer Vision*, 2:7–32, 1990.

[14] J.H. Lambert. Photometria sive de mensura de gratibus luminis, colorum et umbrae. *Eberhard Klett: Augsberg, Germany*, 1760.

[15] H.C. Lee. Method for computing the scene-illuminant from specular highlights. *Journal of Optics Society of America A.*, 3(10):1694–1699, 1986.

[16] H.C. Lee. Illuminant color from shading. In *Perceiving, Measuring and Using Color*, page 1250, 1990.

[17] H.C. Lee, E.J. Breneman, and C.P.Schulte. Modeling light reflection for computer color vision. *IEEE Trans. on Pattern Analysis and Machine Intelligence*, 12:402–409, 1990.

[18] T.M. Lehmann and C. Palm. Color line search for illuminant estimation in real-world scene. *Journal of Optics Society of America A.*, 18(11):2679–2691, 2001.

[19] C. Rosenberg, M. Hebert, and S. Thrun. Color constancy using kl-divergence. In *Internation Conference of Computer Vision*, volume I, page 239, 2001.

[20] S. Shafer. Using color to separate reflection components. *Color Research and Applications*, 10:210–218, 1985.

[21] S. Tominaga. A multi-channel vision system for estimating surface and illumination functions. *Journal of Optics Society of America A.*, 13(11):2163–2173, 1996.

[22] S. Tominaga, S. Ebisui, and B.A. Wandell. Scene illuminant classification: brighter is better. *Journal of Optics Society of America A.*, 18(1):55–64, 2001.

[23] S. Tominaga and B.A. Wandell. Standard surface-reflectance model and illumination estimation. *Journal of Optics Society of America A.*, 6(4):576–584, 1989.

[24] S. Tominaga and B.A. Wandell. Natural scene-illuminant estimation using the sensor correlation. *Proceedings of the IEEE*, 90(1):42–56, 2002.

[25] K.E. Torrance and E.M. Sparrow. Theory for off-specular reflection from roughened surfaces. *Journal of Optics Society of America*, 57:1105–1114, 1966.